ISSN 1995-0780, Nanotechnologies in Russia, 2019, Vol. 14, Nos. 3–4, pp. 125–131. © Pleiades Publishing, Ltd., 2019.
Russian Text © The Author(s), 2019, published in Rossiiskie Nanotekhnologii, 2019, Vol. 14, Nos. 3–4.

FUNCTIONAL AND CONSTRUCTION NANOMATERIALS

Phase Composition Stability of Nanostructured Composite Ceramics Based on CaO–ZrO_2 under Hydrothermal Impact

A. A. Dmitrievskiy[a,*], D. G. Zhigacheva[a], N. Yu. Efremova[a], and A. V. Umrikhin[a]

[a] *Derzhavin Tambov State University, Tambov, 392000 Russia*

**e-mail: aadmitr@yandex.ru*

Received July 22, 2019; revised September 16, 2019; accepted September 16, 2019

Abstract—Structure, phase composition, and mechanical properties (microhardness within indenter penetration depths of 1200 nm ≤ h ≤ 6000 nm and fracture toughness) are studied on nanostructured zirconia ceramics (CaO stabilized) hardened with corundum and SiO_2 during accelerated aging under hydrothermal conditions (T_{ag} = 134°C, P = 3 atm, H = 100%, 0 ≤ t_{ag} ≤ 25 h). The use of CaO as a stabilizer of the zirconia tetragonal phase (instead of "conventional" Y_2O_3) promotes increasing resistance to hydrothermal effects of composite $ZrO_2 + Al_2O_3$ and $ZrO_2 + Al_2O_3 + SiO_2$ ceramics. The reached fracture toughness (more than in 40%) via introduction of silica (C_{SiO_2} = 5 mol %) increase provides a satisfactory hardness/fracture toughness (H = 12.3 GPa, K_C = 6.66 MPa $m^{1/2}$) ratio of the Ca–$ZrO_2 + Al_2O_3 + SiO_2$ composite ceramics even after its accelerated 25-h aging.

DOI: 10.1134/S1995078019020058

INTRODUCTION

Due to the unique complex of mechanical properties; high thermal, chemical, and radiation resistivity; and bioinertness, zirconia ceramics have the widest area of practical applications, from mechanical engineering to medicine. This became possible after discovering the transformational mechanism of its hardening [1], caused by the transition of tetragonal phase t-ZrO_2 (metastable at room temperature) in thermodynamically stable monoclinic phase m-ZrO_2 [1, 2]. This phase transition is accompanied by the change in specific volume (up to 5%) of the mentioned phases and appearance compressive stresses, which prevent the propagation of cracks. Such oxides as Y_2O_3 or CeO_2, rarely MgO, CaO, etc., are usually used as stabilizers of the tetragonal phase at a temperature below the $t \rightarrow m$ transition (T < 1170°C) [3].

Zirconia ceramics have the highest fracture toughness among oxide ceramics (K_C can reach 17 MPa $m^{1/2}$) and relatively low hardness H (to 12–14 GPa) [4]. An increase in one of these characteristics is, as a rule, accompanied by a decreasing in another characteristic. In this regard, to increase the hardness/fracture toughness ratio, ZrO_2 is combined with harder materials. The $ZrO_2 + Al_2O_3$ composites are the most spread; they combine strengths of zirconia ceramics with the advantages of corundum (high hardness H and Young's modulus E) [5–7]. The introduction of nanodispersed corundum particles in zirconia ceramics provides the appearance of the dispersion hardening mechanism in addition to the transformational. The dispersion hardening mechanism is based on the dissipation of energy of a propagating crack as a result of its deviation from the initial direction during a "collision" with harder inclusions (particles) of foreign material (in this case, Al_2O_3 particles) [8–10].

The mechanical characteristics can also be improved by the introduction of the third component (dopant) in the composite ceramics. The dopant additive can promote reducing of the average size and spread of grain size values of ceramic components, prevent the formation of microcracks connected with the difference of linear expansion temperature coefficients on main components of the composite, etc. Thus, in [11] the introduction of SiO_2 in CaO-stabilized zirconium ceramics promotes increasing fracture toughness and hardness of ceramics.

The degradation of ceramics and operating properties under the conditions of increased humidity is the main disadvantage of the zirconia ceramics and composites on which they are based. The degradation of the properties of yttria-stabilized zirconia at 200–300°C was found [12]. Further numerous studies showed that, under prolonged exposure to moisture (even at room temperature), spontaneous $t \rightarrow m$ transition occurs in surface layers. To date, the mechanism of low-temperature degradation of zirconia ceramics is outlined as follows. The filling of oxygen vacancies existing in the ZrO_2 tetragonal phase with hydroxyl ions occurs in a humid atmosphere. This causes the

changing of the local atomic configuration around Zr^{4+} and decreasing the difference between free chemical energy of tetragonal and monoclinic phases. As a result, internal tensile stresses appear and their value reaches 300–500 MPa [13], which leads to the destabilization of the tetragonal phase and its transition to the monoclinic. The most intense $t \rightarrow m$ transition occurs on the grain boundaries where the tensile stresses are maximal. This results in the nucleation and growth of m-ZrO_2 inclusions inside the existing grains of the tetragonal phase. The growth of a part of the monoclinic phase causes a volume expansion, which leads to the cracking of the ceramics along grain boundaries [14]. The formed cracks contribute to the further penetration of moisture and the spread of the transformed zone deep into the material.

The use of other (combining different-valence) stabilizers (CeO_2, CaO) is one possible way of increasing the stability of the phase composition of ceramics under hydrothermal conditions [15, 16]. Another way to prevent low-temperature degradation is reducing tensile stresses on the grain boundaries due to the addition of a small amount of impurities (dopants), which is precipitated at the joints of grains (ternary and higher order) [16]. In this regard, the work is aimed at the investigation of the structure, phase composition, and mechanical properties (microhardness and fracture toughness) on nanostructured composite ceramics $CaO–ZrO_2 + Al_2O_3$ and $CaO–ZrO_2 + Al_2O + SiO_2$ exposed to hydrothermal influences.

EXPERIMENTAL

To prepare the $CaO–ZrO_2 + Al_2O_3$ and $CaO–ZrO_2 + Al_2O_3 + SiO_2$ (CZA and CZAS) composite ceramics, the powders of ZrO_2 (Sigma-Aldrich, USA), Al_2O_3 (Hongwu international group LTD, Hong Kong), CaO (Reachem, Russia), and SiO_2 (Sigma-Aldrich, USA) were used. The molar concentration of stabilizer (CaO) relative to ZrO_2 was kept constant $C_{CaO} = 6.5$ mol %. The part of corundum relative to $CaO–ZrO_2$ was 5.8 mol %. To produce the CZAS samples, a SiO_2 additive (5 mol %) was introduced to the mixture. According to [10, 17], the ratios of the component concentration provide a high ratio of hardness and fracture toughness of the studied composite ceramics.

The powder mixtures were dispersed in distilled water (in a mass ratio of 1:3) using ultrasound. Then, the mixture was milled in a Pulverisetter 7 Premium Line (Fritsch, Germany) planetary mill for 5 h with balls 1.5 mm in diameter with accelerating movement at 65g. After the milling, the mixture was dried in a furnace at $T_0 = 80$°C for 24 h. The formation of samples was performed via uniaxial dry pressing at a load of 500 MPa for 20 min.

The samples were sintered in a two-stage mode at air atmosphere. On the first stage, the samples were heated to $T_1 = 1300$°C with a constant rate (5°C/min) and held for 5 min. Then, samples were cooled to $T_2 = 1200$°C and sintered for 4 h. According to [18], this ratio of the temperatures of two-stage sintering mode is optimal for $CaO–ZrO_2 + Al_2O_3$ ceramics with low corundum content in terms of its mechanical properties. To study the mechanical characteristics, the prepared samples were mechanically ground and polished.

Hydrothermal (accelerated) aging was carried out in an autoclave with pressure and temperature control. The temperature was maintained within $T_{ag} = 132–134$°C. The pressure of saturated steam at these temperatures is ~3 atm. According to [19], exposure in these conditions for 1 h corresponds to three to four years of aging in natural conditions. The maximal exposure time of the samples under mentioned conditions reached 25 h, which corresponds to 75–100 years of natural aging.

The $P–h$ diagrams (P is indenter load and h is indenter penetration depth) in the mode of five-cycle loading (Berkovich pyramid) were registered using a NanoIndenter G200 nanoindentometer (MTS NanoInstruments, USA). To estimate the fracture toughness via indentation method, a Duramin-A300 automated microhardness tester (EmcoTest, Austria) with the Vickers pyramid was used. In this case, the hardness was tested under loads of 50 N, which corresponds to the depth of indenter penetration of $h \sim 12$ μm. When the indenter loads are smaller, the size of radial cracks formed in the corners of the indentation does not allow the estimation of K_C value. An Axio Observer A1m inverted metallographic microscope with a Struktura 5.0 image analyzer was used for the visualization of indenter imprint and measurements of radial cracks formed in the area of indenter imprint. The value of fracture toughness K_C was determined according to [20] using the following equation:

$$K_C = 0.016\left(\frac{E}{H}\right)^{\frac{1}{2}}\frac{P}{l^{\frac{3}{2}}}, \quad (1)$$

where P is a maximal load on the indenter (50 N), and l is a length of radial cracks near the imprint. The phase composition was determined via X-ray diffraction (XRD) analysis using a D2 Phaser diffractometer (Bruker AXS, Germany); phase content was estimated via Rietveld method. The structure of composite ceramics was visualized using a Merlin scanning electron microscope with high resolution (Carl Zeiss, Germany).

RESULTS AND DISCUSSION

The content of the monoclinic phase ($C_{m\text{-}ZrO_2}$) in zirconia ceramics having high mechanical properties

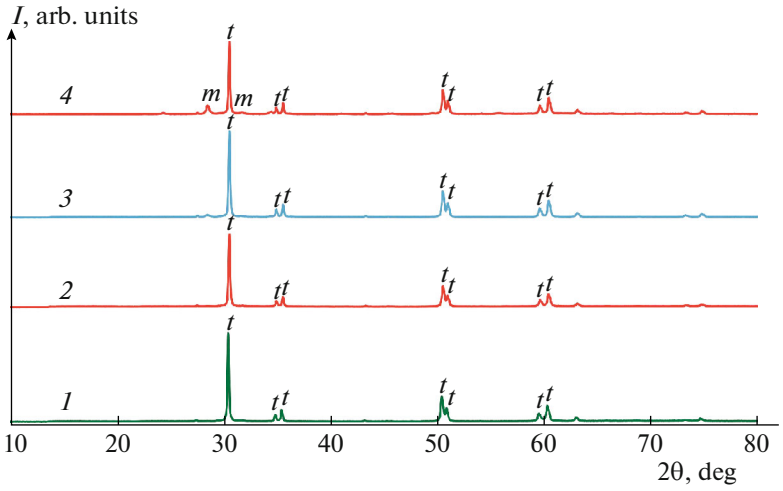

Fig. 1. (Color online) XRD patterns recorded on initial (*1* and *3*) and aged at t_{ag} = 25 h (*2* and *4*) samples of $CaO–ZrO_2 + Al_2O_3$ (*1* and *2*) and $CaO–ZrO_2 + Al_2O_3 + SiO_2$ (*3* and *4*).

usually does not exceed a few percents. According to X-ray diffraction analysis data, the content of the *m*-phase of zirconia in CZA and CZAS samples did not exceed 2 and 3%. The exposure of the CZA samples for 25 h under hydrothermal conditions does not cause noticeable (taking into account the measurement error) changes to $C_{m\text{-}ZrO_2}$. Silicon-containing CZAS samples demonstrate lower resistance to aging. As an example, the XRD patterns of the initial and aged CZA and CZAS samples are given in Fig. 1. The spectrum of the aged CZAS sample contains peaks corresponding to the monoclinic phase of zirconia.

The results of the analysis of the XRD patterns recorded at different aging stages are given in Fig. 2 as the dependence of the concentration of the monoclinic zirconia phase on the duration of aging $C_{m\text{-}ZrO_2}(t_{ag})$. The hydrothermal treatment of CZAS samples, the growth of *m*-phase content to the values of $C_{m\text{-}ZrO_2}$ = 8% is observed during first 5 h (Fig. 2, curve *2*). Note, that the content of tetragonal phase $C_{t\text{-}ZrO_2}$ synchronously decreases. At further treatment of CZAS samples, the $C_{m\text{-}ZrO_2}(t_{ag})$ dependences flatten, and, at the maximal duration of accelerated aging (t_{ag} = 25 h), part of the *m*-phase does not exceed the value of $C_{m\text{-}ZrO_2}$ = 12%. Part of the cubic phase of zirconia in CZA and CZAS samples fluctuates between 2 to 8% during hydrothermal treatment.

The dependences of the content of the zirconia monoclinic phase on the duration of the accelerated aging (under the same conditions) for the samples of Y_2O_3-stabilized zirconia (YSZ) (Fig. 2, curve *3*) and composite ceramics based on YSZ and corundum in the ratio of 50 : 50% (Fig. 2, curve *3*) are given for comparison; the curves of the abovementioned ceramic sample were adapted from [19] and [21]. Even the CZAS samples degrading during the accelerated aging demonstrate significantly higher resistance to the hydrothermal effect compared with the YSZ and YSZ-corundum composite.

Taking into consideration the abovementioned mechanism of the low-temperature degradation, the moisture impact could reduce the mechanical properties. We must take into account that the thickness of the degraded layer is proportional to the aging duration [22]. Hence, in the early stages of aging (at a small thickness of the degraded layer), the changes in hardness can depend on the thickness of the tested layer

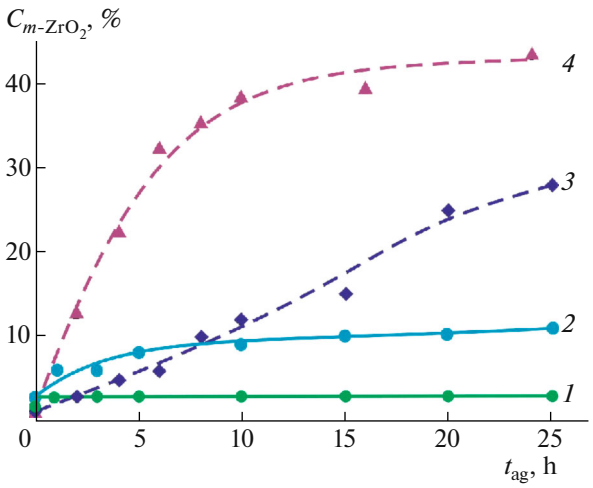

Fig. 2. (Color online) Dependences of a part of zirconia monoclinic phase on the time of accelerated aging for the $CaO–ZrO_2 + Al_2O_3$ (*1*), $CaO–ZrO_2 + Al_2O_3 + SiO_2$ (*2*), $Y_2O_3–ZrO_2$ (*3*), and $Y_2O_3–ZrO_2 + Al_2O_3$ (*4*) samples. Curves *3* and *4* are adapted from [19, 21].

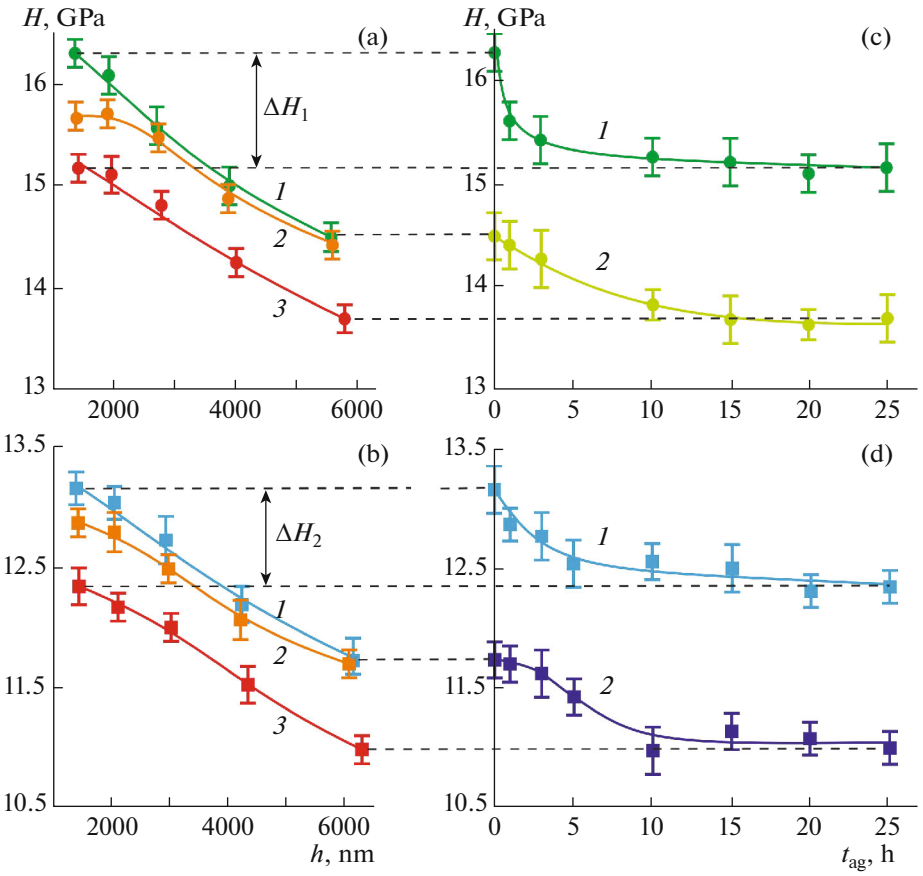

Fig. 3. (Color online) Dependences of hardness of the indenter penetration depth (a, b) and time of accelerated aging (c, d) for the $CaO–ZrO_2 + Al_2O_3$ (a, c) and $CaO–ZrO_2 + Al_2O_3 + SiO_2$ (b, d) samples. (a, b) *1*—initial samples; *2*—samples aged at t_{ag} = 1 h; *3*—samples aged at t_{ag} = 25 h. (c, d) Curves at indenter penetration depth of (*1*) h_1 ~ 1200 nm and (*2*) h_5 ~ 6000 nm.

(the depth of indenter penetration). In this regard, the method of five-cycle loading, which allows determination of H value on the different depth of the indenter penetration (from h_1 ~ 1200 to ~ 6000 nm), was used during study of the effect of accelerated aging on the hardness of CZA and CZAS ceramics. The hardness value of the CZA and CZAS initial samples decreases as the depth of indenter penetration increases (Fig. 3a and 3b, curves *1*). This behavior of the $H(h)$ dependence is characteristic for most of the materials and caused by the size effects in micro- and nanocontacts [23].

The $H(h)$ dependences for the CZA and CZAS samples aged for 1 and 25 h (curves *2* and *3*) are given in Fig. 3. One hour aging in hydrothermal conditions (t_{ag} = 1 h) causes a highly noticeable (taking into account measurement error) change of hardness measured at indenter penetration depth (h_1) at ~1200 nm. Increasing of indenter penetration depth leads to a gradual decrease in the difference of H values of initial and aged (t_{ag} = 1 h) samples (Fig. 3a, curves *1* and *2*). When h_5 ~ 6000 nm, the difference in H values of initial and aged samples totally disappears, i.e., the thickness of the degraded (t_{ag} = 1 h) layer is much less than the thickness of the tested layer.

An increase in the aging duration is accompanied by the growth of the thickness of the degraded layer. The H changes of both types of samples (CZA and CZAS) caused via aging (t_{ag} = 25 h) are observed in the whole studied range of indenter penetration depth (Figs. 3a and 3b, curves *1* and *3*). This indicates that during 25 h of aging, the thickness of the degraded layer becomes commensurate with the maximal (in this experiment conditions) depth of indenter penetration (h_5 ~ 6000 nm). Figures 3c and 3d demonstrate the brought into correspondence dependences of hardness H measured at h_1 ~ 1200 nm (curves *1*) and h_5 ~ 6000 nm (curves *2*) on aging time t_{ag} for CZA and CZAS samples. The $H(t_{ag})$ dependences have saturation independently on the depth of indenter penetration. The softening value does not exceed the ΔH_1 = 8% and ΔH_2 = 6.5% for samples CZA and CZAS; this

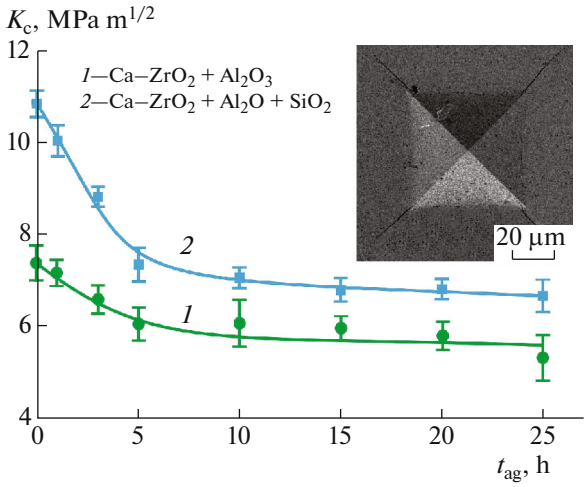

Fig. 4. (Color online) Dependences of fracture toughness K_C on the duration of accelerated aging of (*1*) CaO–ZrO_2 + Al_2O_3 and (*2*) CaO–ZrO_2 + Al_2O_3 + SiO_2 samples in hydrothermal conditions t_{ag}. The insert presents characteristic SEM image of the indenter imprint in the initial (before aging) sample CaO–ZrO_2 + Al_2O.

indicates the high resistance of mechanical properties (nano- and microhardness) of the developed composition ceramics to aging in hydrothermal conditions. The "rate" of the weakening observed at the aging (angle of $H(t_{ag})$ dependence on the initial aging stages) depends on the depth of the indenter penetration. This imposes requirements for the obligatory indication of H testing conditions (the type of indenter and the maximum depth of its penetration) at studying the effect of hydrothermal effects on the mechanical properties of zirconium ceramics and composites on which it is based.

The hardness/fracture toughness ratio is of great importance for fragile materials. In this regard, the effect of accelerated aging on the K_C value of CZA and CZAS samples was studied additionally. A characteristic SEM image of the indenter imprint with radial cracks formed in the initial (not hydrothermally exposed) CZA sample is given in Fig. 4 (insert).

During the first 5 h of the accelerated aging, the K_C value decreases for both types of samples. However, when $t_{ag} > 5$ h, the $K_C(t_{ag})$ dependences become flat (Fig. 4). A steeper $K_C(t_{ag})$ dependency slope is characteristic for the CZAS samples within $0 < t_{ag} < 5$ h and, consequently, there is a more significant (~38%) decrease in fracture toughness. The martensitic $t \rightarrow m$ transformation of zirconia observed at the same time range of the accelerated aging (Fig. 2) is the most probable cause of enhancement of the degradation of fracture toughness of the CZAS samples.

The degradation of phase composition of the near-surface layers of the studied samples, which is caused by hydrothermal effects, affects the process of local deformation under concentrated loads (in particular, on the structure of the formed indenter imprint). Fig. 5 demonstrates characteristic SEM images of surface areas (edge of the indenter imprint and a part of radial cracks) of CZA and CZAS samples. The imprints of indenter (Vickers pyramid) were formed on the initial samples (Figs. 5a and 5b) and after their accelerated aging for $t_{ag} = 25$ h (Figs. 5c and 5d).

At indentation of the samples without hydrothermal treatment, pronounced single radial cracks form. The hydrothermal treatment of the samples ($t_{ag} =$ 25 h) causes the appearance of "chipping" of the

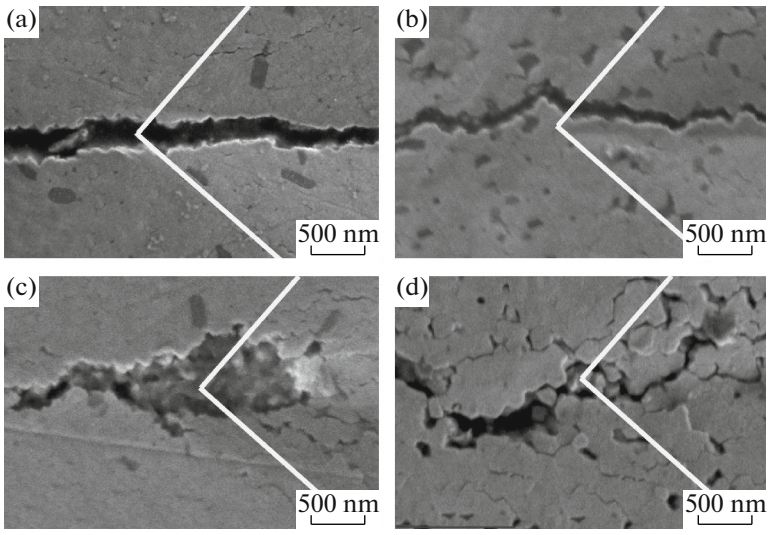

Fig. 5. Characteristic SEM images of the surface areas of the (a, b) initial and (c, d) after accelerated aging at 25 h of (a, c) CaO–ZrO_2 + Al_2O_3 and (b, d) CaO–ZrO_2 + Al_2O_3 + SiO_2 samples. White lines indicate the boundaries of the indenter imprints.

material in the edges of the imprint. A dense structure of sintered zirconia and corundum crystallites maintains in the imprint internal surface of the initial samples. Hydrothermal treatment leads to the appearance of "cracking" along the grain boundaries inside the indenter imprint. The destructive effect of moisture is observed to a greater extent in the CZAS samples, which demonstrate a higher decreasing of fracture toughness at accelerated aging.

Thus, the combining zirconia with corundum provides the simultaneous appearance of two hardening mechanisms: transformational and dispersion. A decrease of a relative part of the tetragonal t-ZrO_2 phase during low-temperature degradation, which is usually observed in YSZ ceramics, causes the reducing of a part of the transformational hardening mechanism. However, the dispersion hardening mechanism retains its role and prevents the degradation of the mechanical properties of composite ceramics.

We note that the high resistivity of the phase composition of CZA samples (Fig. 2) in hydrothermal conditions is reached due to the use of CaO as the stabilizer of t-ZrO_2 tetragonal phase; the optimal concentration C_{CaO} is 6.5 mol % [16, 24]. The observed decrease in the part of the t-ZrO_2 tetragonal phase during the accelerated aging of CZAS samples (Fig. 2, curve *2*) is likely caused by reducing a relative part of the stabilized because of the formation of calcium silicate. Under the hydrothermal conditions, the process of the formation of $CaSiO_3$ and Ca_2SiO_4 is more intense, which is accompanied by the imbalance in the ratio of ZrO_2 and CaO concentrations and, as a result, should lead to the reducing of mechanical properties.

On the other hand, as noted in [25], the introduction of silica in zirconium ceramics promotes the process of its sintering, which positively affects its mechanical properties. Moreover, according to the comparative analysis of XRD patterns (Fig. 1), the introduction of SiO_2 in CZA ceramics does not cause the appearance of new lines in spectra recorded for the initial and aged samples. This indicates the absence of crystalline silica and calcium silicate in CZAS samples. The introduced silica and formed calcium silicate likely exist in the amorphous state and are distributed by a thin layer along the grain boundaries of ZrO_2 and Al_2O_3. A similar conclusion was made by the authors of [11] during studies on the effect of SiO_2 content on phase compositions and mechanical properties of $CaO–ZrO_2$ ceramics. The formation of amorphous SiO_2, $CaSiO_3$, and Ca_2SiO_4 on grain boundaries of ZrO_2 and Al_2O_3 and their junctions (ternary or higher order) leads to the decreasing of mechanical stresses [26]. This also positively affects the value of the fracture toughness.

CONCLUSIONS

The introduction of SiO_2 in zirconium ceramics hardened by corundum allows increasing fracture toughness more than in 40% while the hardness decreases lower than in 20%. The use of CaO as the stabilizer of the zirconia tetragonal phase in oxide ceramics ZrO_2 Al_2O_3 and $ZrO_2 + Al_2O_3 + SiO_2$ allows significant increase in the resistance of phase composition of mechanical properties (hardness and fracture toughness) to low-temperature degradation.

Thus, the proposed technology of preparation of composite ceramics based on zirconia allows increasing its life use in hydrothermal conditions.

ACKNOWLEDGMENTS

The authors are grateful to A.O. Zhirachev for assisting in obtaining SEM images. This work was carried out using Shared Access Center of Derzhavin Tambov State University facilities.

FUNDING

The work was supported by the Ministry of Science and Education of the Russian Federation (project no. 16.2100.2017/4.6) and partially supported by the Russian Foundation for Basic Research (project no. 18-42-680001 r-a).

REFERENCES

1. R. C. Garvie, R. H. J. Hannink, and R. T. Pascoe, Nature (London, U.K.) **258**, 703 (1975). www.nature.com/articles/258703a0.pdf.
2. R. H. J. Hannink, P. M. Kelly, and B. C. Muddle, J. Am. Ceram. Soc. **83**, 461 (2000). https://doi.org/10.1111/j.1151-2916.2000.tb01221.x
3. A. C. O. Lopes, P. G. Coelho, L. Witek, et al., Ceram. Int. **45**, 8840 (2019). https://doi.org/10.1016/j.ceramint.2019.01.211
4. A. O. Zhigachev, Yu. I. Golovin, A. V. Umrikhin, et al., *Zirconia Dioxide Ceramic Materials* (Tekhnosfera, Moscow, 2018) [in Russian].
5. A. G. Evans, J. Am. Ceram. Soc. **72**, 187 (1990). https://doi.org/10.1111/j.1151-2916.1990.tb06493.x
6. M. H. Ghaemi, S. Reichert, A. Krupa, et al., Ceram. Int. **43**, 9746 (2017). https://doi.org/10.1016/j.ceramint.2017.04.150
7. A. Maji and G. Choubey, Mater. Today: Proc. **5**, 7457 (2018). https://doi.org/10.1016/j.matpr.2017.11.417
8. J.-K. Lee, M.-J. Kim, and E.-G. Lee, J. Mater. Sci. Lett. **21**, 259 (2002). https://doi.org/10.1023/A:1014737614591
9. F. Zhang, L.-F. Li, and E.-Z. Wang, Ceram. Int. **41**, 12417 (2015). https://doi.org/10.1016/j.ceramint.2015.06.081

10. A. A. Dmitrievskii, A. O. Zhigachev, D. G. Zhigacheva, and A. I. Tyurin, Tech. Phys. **64**, 86 (2019). https://doi.org/10.21883/JTF.2019.01.46970.102-18
11. A. O. Zhigachev, V. V. Rodaev, A. V. Umrikhin, and Yu. I. Golovin, Ceram. Int. **45**, 627 (2019). https://doi.org/10.1016/j.ceramint.2018.09.220
12. K. Kobayashi, H. Kuwajima, and T. Masaki, Solid State Ionics **3–4**, 489 (1981). https://doi.org/10.1016/0167-2738(81)90138-7
13. H. Schubert and F. Frey, J. Eur. Ceram. Soc. **25**, 1597 (2005). https://doi.org/10.1016/j.jeurceramsoc.2004.03.025
14. Y. Gaillard, E. Jimenez-Pique, F. Soldera, et al., Acta Mater. **56**, 4206 (2008). https://doi.org/10.1016/j.actamat.2008.04.050
15. J.-D. Lin, J.-G. Duh, and C.-L. Lo, Mater. Chem. Phys. **77**, 1016 (2002). https://doi.org/10.1016/S0254-0584(02)00161-X
16. A. O. Zhigachev and Yu. I. Golovin, Nanotechnol. Russ. **12**, 400 (2017). https://nanorf.elpub.ru/jour/article/view/12/11.
17. A. A. Dmitrievskii, D. G. Zhigacheva, A. I. Tyurin, et al., in *Proceedings of the International Symposium on Perspective Materials and Technologies, May 27–31, 2019, Brest, Belorussiya*. http://www.issp.ac.ru/ebooks/conf/Adv.mater_2019.pdf.
18. A. A. Dmitrievskii, A. I. Tyurin, A. O. Zhigachev, D. G. Guseva, and P. N. Ovchinnikov, Tech. Phys. Lett. **4**, 141 (2018). https://doi.org/10.21883/PJTF.2018.04.45635.16933
19. J. Chevalier, S. Deville, E. Münch, et al., Biomaterials **25**, 5539 (2004). https://doi.org/10.1016/j.biomaterials.2004.01.002
20. A. Moradkhani and H. Baharvandi, Eng. Fract. Mech. **191**, 446 (2018). https://doi.org/10.1016/j.engfracmech.2017.12.033
21. M. P. Albano, H. L. Calambás Pulgarin, L. B. Garrido, et al., Ceram. Int. **42**, 11363 (2016). https://doi.org/10.1016/j.ceramint.2016.04.063
22. T. Kosmač and A. Kocjan, J. Eur. Ceram. Soc. **32**, 2613 (2012). https://doi.org/10.1016/j.jeurceramsoc.2012.02.024
23. Yu. I. Golovin, Phys. Solid State **50**, 2205 (2008). http://journals.ioffe.ru/articles/viewPDF/2862.
24. A. O. Zhigachev, A. V. Umrikhin, and Yu. I. Golovin, Ceram. Int. **41**, 13804 (2015). https://doi.org/10.1016/j.ceramint.2015.08.063
25. M. L. Mecartney, J. Am. Ceram. Soc. **70**, 54 (1987). https://doi.org/10.1111/j.1151-2916.1987.tb04853.x
26. L. Gremillard, J. Chevalier, T. Epicier, and G. Fantozzi, J. Am. Ceram. Soc. **85**, 401 (2002). https://doi.org/10.1111/j.1151-2916.2002.tb00103.x

Translated by N. Saetova